Title:

Crystal structure of a Photosystem II-related, Manganese-binding, TPM-domain protein at a 1.6 Å resolution

Authors:

André Vidal-Meireles[1]; Soazig Malesinski[1]; Yann Horrenberger[1]; Caroline Monteil[1]; Jean Alric[1]; Marina Siponen[1]; Xenie Johnson[1]

[1]Aix Marseille Univ, CEA, CNRS, BIAM, UMR7265, Saint-Paul-Lez-Durance, France

Abstract:

Conserved proteins across oxygenic phototrophic organisms are important players in photosynthetic acclimation, yet many remain poorly or completely uncharacterized. In the green alga *Chlamydomonas reinhardtii* we identified Cre15.g636050, previously annotated as *CPLD31*, that encodes such an uncharacterized, conserved, thylakoid lumenal protein belonging to the “TPM” domain family (PF04536). TPM refers to a protein fold named after the three founding proteins of this family, TLP18.3, Psb32, and MOLO-1, with the first two being Photosystem II-related proteins. We also found a paralogue of *CPLD31*, Cre03.g154600, previously annotated as *TLP15.2*. In this work, we generated knock-out mutants of these genes in Chlamydomonas and produced the recombinant proteins. We showed both proteins are regulated by light and phototrophy, and while the former binds manganese in a TPM-domain metal binding site, the latter does not.
Therefore, we reannotated them as **L**umenal **M**n-binding **T**PM-domain **P**rotein **1** (LMTP1) and **T**hylakoid **L**umenal **P**rotein **26** kDa (TLP26), respectively.

Keywords:

Crystal structure; Thylakoid lumen; Photosystem II; Manganese; TPM domain; Sll1071; CPLD31; At5G52970; TLP15; LMTP1; TLP26.

Introduction

Under high light stress, Photosystem II (PSII) can become damaged due to the generation of reactive oxygen species (ROS), particularly at the level of D1 (Didaran et al., 2024). The repair of D1 subunits is a tightly regulated process that involves migration of PSII from grana to the stromal lamellae, before D1 degradation and replacement by a new subunit (Baena–González and Aro, 2002). Different redox-regulated lumenal proteins participate in this process, including proteases (such as FtsH and Deg) and immunophilins (Järvi et al., 2013). Immunophilins are a group of two different families of proteins (annotated as either CYPs or FKBPs) highly abundant in the lumen, that mediate the maintenance and turnover of PSII, Cytochrome b_6f, and Photosystem I (He et al., 2004). Although canonical immunophilins are characterized by having a PPIase activity, which facilitates protein folding by an interaction with proline residues, CYPs and FKBPs from the thylakoid lumenal space typically have lost that activity (Shapiguzov et al., 2006). One of the best characterized immunophilins from the lumen without PPIase activity is CYP38 from *A. thaliana* (Fu et al., 2007; Sirpiö et al., 2008).

In *Δcyp38* plants, which have stunted growth and show accumulation of reactive oxygen species, the levels of D1 are diminished, as well as the amount of PSII super complexes (Fu et al., 2007). Additionally, the phosphorylation levels of D1, D2, and LHCIIs are increased in these mutants, suggesting that CYP38 plays a role in the regulation of the phosphorylation state of these proteins (Sirpiö et al., 2008). CYP38 is divided in two main domains, an N-terminal domain that is proposed to control an autoinhibitory mechanism of CYP38, and a C-terminal domain that may be responsible for the catalytic function of this immunophilin as a chaperone for different lumenal targets working as protein complexes (Vasudevan et al., 2012). Using an *A. thaliana* thylakoid lumen library for yeast-two-hybrid screenings, 15 soluble and membrane-bound protein candidates were proposed to assist CYP38 in the regulation of PSII assembly and repair via interaction with the C-terminal domain (Hao et al., 2021). Two proteins of the TPM-domain family of proteins could be identified amongst the candidate proteins: TLP18.3 and the uncharacterized protein AtTLP15.

The TPM-domain superfamily of proteins is named after the three founding proteins of this domain: **T**LP18.3, **P**sb32, and **M**OLO-1; formerly known as DUF477, this family of proteins is broadly conserved in prokaryotic and eukaryotic organisms, and it is characterized by a conserved secondary structure (a central hydrophobic β-sheet, made of four β-strands, flanked by four amphiphilic α-helices), even though the aminoacid sequence between different TPM-domain proteins is rather variable (Eletsky et al., 2012; Cerutti et al., 2017). TLP18.3 is involved in PSII repair at the level of D1 turnover, as

Δtlp18.3 mutants from Arabidopsis have slower D1 degradation rates (Sirpiö et al., 2007); the cyanobacterial homologue of TLP18.3, Psb32, also plays a similar role in PSII repair during high light acclimation. These proteins are not regarded as essential subunits of PSII, as mutants of those proteins are still viable, but rather as accessory proteins required to confer fitness and aid in the process of acclimation (Sirpiö et al., 2007; Wegener et al., 2011).

Given that all proteins in the TPM domain family share a similarly organized domain (Pellizza et al., 2016), it is plausible that other proteins in the thylakoid lumen possessing a TPM domain may also play a role in the regulation of PSII. TLP15, part of a subfamily of TPM-domain containing proteins (PTHR35514 / Thylakoid_lumenal_15kDa-like), came to our attention because a bioinformatics approach predicts its conservation across all oxygenic phototrophic organisms and associates its conservation with PSII (Chazaux et al., 2020). The green algae *Chlamydomonas reinhardtii* encodes two putative paralogues of this family of proteins, one encoded by Cre15.g636050 and annotated as CPLD31, and another encoded by Cre03.g154600, annotated as TLP15.2.

Based on the atomic resolution of the 3D structure of CPLD31, and functional findings within this manuscript, we propose that the two paralogues are distinct proteins that evolved from a common, cyanobacterial, ancestor. Thus, the annotation of these proteins was updated to **L**umenal **M**n-binding **T**PM-domain **P**rotein **1** (LMTP1) and **T**hylakoid **L**umenal **P**rotein **26** kDa (TLP26), respectively. Part of the findings reported in this manuscript were presented as a poster in the Second European Congress on Photosynthesis Research (Vidal-Meireles et al., 2024).

Results

Genomics is a powerful tool to analyze the origins of oxygenic photosynthesis and predict which genetic factors could be the most relevant to photoprotection and the control of photosynthetic yields (Mulkidjanian et al., 2006; Merchant et al., 2007; Heinnickel and Grossman, 2013; Beck et al., 2018). A coarse filtering of all oxygenic phototrophs sequenced to date identified some 85 gene families split into 50 genes coding for known protein subunits and regulators of the photosynthetic apparatus, and another 35 gene families with unknown function (Mulkidjanian et al., 2006). In (Chazaux et al., 2020) we applied a fine filter to this subgroup, by comparison against the cyanobacterial genomes analyzed by (Beck et al., 2018) where we searched for conserved genes that have evolved

with photosynthesis but were lost in the cyanobacterial accessions that have lost PSII. In this analysis we identified *slr0575* and *sll1071* in *Synechocystis* sp. PCC 6803. The Chlamydomonas homologue of *sll1071* at chromosome 15, Cre15.g636050, was annotated as *Conserved in the Green Lineage and Diatoms 31* (*CPLD31*). We identified a paralogue of Cre15.g636050 in the green alga genome at chromosome 3, Cre03.g154600, annotated as *Thylakoid Lumenal 15.0 kDa Protein 2* (*TLP15.2*). Our work on the function and localization of these proteins went along with reannotating Cre15.g636050 as **L**umenal **M**n-binding **T**PM-domain **P**rotein **1** (LMTP1) and Cre03.g154600 as **T**hylakoid **L**umenal **P**rotein **26** kDa (TLP26). These annotations are consistently used throughout the manuscript.

Generation of C. reinhardtii Δlmtp1 and Δtlp26 mutants via CRISPR/Cas9

No mutants were available in the CLiP library (Li et al., 2019) with a clear insertion in the coding region of either target genes, so we generated *C. reinhardtii Δlmtp1* (encoded by Cre15.g636050) and *Δtlp26* (encoded by Cre03.g154600) mutants via CRISPR/Cas9. The first exons of each gene were targeted using *in vitro* assembled RNP particles. Based on bioinformatics predictions (Naito et al., 2015; Concordet and Haeussler, 2018) for Cre15.g636050, we selected CCTCGGCACGCTGGAAGTTACGG, located at the 5'UTR of the gene's first exon, as the sole target, while for Cre03.g154600 two targets were selected, CAAATGGCAGCGAGCTACAGCGG at the 5'UTR of the gene's first exon and AGTTGAGCTTGTCACGCTTGCGG at the second exon (Fig. 1a). Gene disruption was confirmed using a PCR-based approach, using primers upstream and downstream of the target site (Figure 2b).

Antibodies against LMTP1 and TLP26 were raised, using recombinant proteins produced in *E. coli* (full-length for LMTP1 and without predicted transmembrane helices for TLP26 – see Supplemental Figure 1a), which we show are specific to their paralogue (Figure 1c). The *Δlmtp1* and *Δtlp26* CRISPR mutants confirmed that the LMTP1 antibody is very specific against total protein extracts of *C. reinhardtii*, showing a single band around 17kDa in the WT strain which is completely absent from the *Δlmtp1* mutant. The antibody raised against TLP26 shows several unspecific bands, one of which is missing in the *Δtlp26* mutants, at around 26kDa, which is the predicted protein molecular weight (Figure 1d).

Both LMTP1 and TLP26 are predicted to be localized in the thylakoid lumen using TargetP 2.0 (Almagro Armenteros et al., 2019), with DeepTMHMM (Hallgren et al., 2022) predicting LMTP1 to be a soluble protein and TLP26 to have three C-terminus transmembrane α-helices (Supplemental Figure 1a). Additionally, using a Venus-tagged

144 construct, LMTP1 has been shown to co-localize mostly to the chloroplast of *C. reinhardtii*
145 (Wang et al., 2023). To show the chloroplast localization of TLP26, we performed
146 immunoblot analyses on isolated thylakoids, where no signal was detected for LMTP1,
147 and a clear signal was visible for TLP26 (Figure 1e).
148
149 <u>*LMTP1 and TLP26 likely plays a regulatory role during photosynthetic acclimation*</u>
150 Sll1071 and LMTP1 have been predicted as regulators of PSII activity in *Cyanobacteriota*
151 (former *Cyanobacteria*) and plants in previous bioinformatics and proteomics analyses
152 (Mulkidjanian et al., 2006; Dahlgren et al., 2021; Hao et al., 2021). We also suggest they
153 are similar to other auxiliary proteins highly conserved in oxygenic phototrophs. Like APE1,
154 TLP18.3, and Psb32 (Sirpiö et al., 2007; Wegener et al., 2011; Chazaux et al., 2020), they
155 are required for photosynthetic acclimation rather than being constitutive subunits of PSII
156 or essential biogenesis proteins. To evaluate the accumulation levels of both LMTP1 and
157 TLP26 during acclimation to photoautotrophic conditions, and to determine if these
158 proteins are essential for PSII activity, we grew WT *C. reinhardtii* cells under
159 photomixotrophic conditions (TAP medium) with 20 μmol photons$\cdot m^{-2} \cdot s^{-1}$ illumination
160 before shifting them into photoautotrophic conditions (MIN medium) with 40 μmol photons$\cdot$
161 $m^{-2} \cdot s^{-1}$ illumination for 4 days, and then for 250 μmol photons$\cdot m^{-2} \cdot s^{-1}$ for additional 3 days.
162 At each time-point samples were collected for protein isolation on whole cells extracts,
163 which were then analyzed via immunoblotting. We have observed that both proteins
164 accumulate constitutively in *C. reinhardtii*, and that LMTP1 accumulation increases upon
165 a shift to photoautotrophic conditions and TLP26 accumulation increases upon a shift to
166 high light (Figure 2a). Under photoautotrophic conditions and moderate light illumination
167 *Δlmtp1* and *Δtlp26* divide at a rate similar to WT (with an exponential division rate of around
168 4 days for cells grown in MIN medium at 40 μmol photons$\cdot m^{-2} \cdot s^{-1}$ illumination), and their
169 photosynthetic Chl *a* fluorescence parameter F_V/F_M was the same as the WT (Figure 2b).
170 When analyzing circadian regulation data from *C. reinhardtii* datasets (Zones et al., 2015),
171 we observe that *LMTP1* transcripts follow a circadian rhythm similarly observed for
172 *TLP18.3*: the transcript abundance increases from dawn to the middle of the day,
173 decreasing then to a basal level that is maintained during the night-period. On the other
174 hand, *TLP26* transcript abundance follows a different trend, in the same group of genes
175 such as those involved in the accumulation of antioxidant species such as Vitamin C: at
176 dawn, *TLP26* mRNA transcript abundance spikes, and then quickly decreases to a basal
177 level that is close to the detection limit (Figure 2c). This suggests that while both proteins
178 may be involved in photosynthetic acclimation, they are implied in different processes.

179

180 *The crystal structure of recombinant LMPT1 and fluorescence measurements reveals a*
181 *TPM-domain metal-binding site*

182 Although some progress has been made in the understanding of the cellular role of TPM-
183 containing proteins, the relationship between structure and function is not clear. While
184 several structures have been elucidated, there appears to be no consensus on the role of
185 TPM-domain containing proteins, nor is there a single clearly attributable function to the
186 structural motif that is a TPM-domain. The structure of six TPM domain containing proteins
187 have been determined either by X-ray crystallography or NMR: BA42 from *Bizionia*
188 *argentinensis* [PDB codes: 2MPB and 4OA3], BA41 from *B. argentinensis* [PDB code:
189 5ANP], TLP18.3 from *Arabidopsis thaliana* [PDB code: 3PTJ] (Wu et al., 2011; Aran et al.,
190 2014; Cerutti et al., 2017), and Rhom172_1776 from *Rhodothermus marinus* [PDB code:
191 7TBR], CG2496 from *Corynebacterium glutamicum* [PDB code: 2KPT], and PG0361 from
192 *Porphyromonas gingivalis* [PDB code: 2KW7 (all unpublished structures at the time of this
193 submission).

194 To gain more insights into the molecular function of LMTP1, we obtained crystals
195 and performed X-ray diffraction experiments, which were complemented with fluorescence
196 measurements on the recombinant protein. Recombinant tagged proteins were purified
197 using affinity chromatography, followed by cleavage of the His-tag and size exclusion
198 chromatography (SEC). A buffer range from pH 5 to pH 7 was tested by thermal melting
199 with optimal stability obtained in a 20 mM MES,150 mM NaCl buffer at pH 6.5. This buffer
200 was therefore used for further SEC purifications and *in vitro* characterization. Recombinant
201 proteins were obtained at a final concentration of about 1 mg/ml and further concentrated
202 to 6 mg/ml for protein crystallography. Crystal screening results revealed 0.2 M $CaCl_2$, 0.1
203 M HEPES/KOH (pH 7.0), and 20% PEG 6000 as the most successful and reproducible
204 condition for obtaining needle-like crystals. The successfully obtained LMTP1 crystals
205 were resolved by X-ray diffraction at 1.6 Å (Figure 3). The crystal structure presents with
206 a near canonical TPM fold – a central hydrophobic β-sheet, made of four β-strands, flanked
207 by amphiphilic α-helices on each side (Cerutti et al., 2017). Interestingly, the secondary
208 structure motifs present in this structure are generally shorter than in the canonical fold,
209 resulting in a structure with generally more loop structures. Additionally, the LMTP1
210 structure contains a metal co-factor binding site in a region which is generally structurally
211 conserved in other TPM-domain proteins, but which is mostly uncharged in other
212 structures. Using Alphafold3 (Abramson et al., 2024), we predicted a similar fold and metal
213 binding site to our recombinant LMTP1 structure (Supplemental Figures 1b and 1c).

214 As mentioned, the structure of LMTP1 shows a near canonical TPM fold with a
215 three-layered α/β architecture composed of a four-stranded β-sheet flanked by four of the
216 five helices present in the structure. Three α-helices are present on one side and a single
217 small helix on the other side of the β-sheet which runs from the N-terminus through to the
218 C-terminus with the topology A(↑)B(↑)C(↑)D(↓). α-Helices I, IV, and V are packed
219 against one side of the β-sheet, while α-helix II is located on the opposite side, constituting
220 an αβα sandwich structure. α-Helix III is perpendicular to the plane of the β-sheet, which
221 represents the middle layer of the sandwich. The locations of all these regular secondary
222 structure elements are: β-strands A (residues 95-98), B (125-127), C (169-176), and D
223 (163-167), and α-helices I (102-121), II (138-144), III (179-188), IV (191-196), and V (198-
224 214). A notable difference in the αβα sandwich structure is in the "lack of substance" in the
225 second α-layer of the sandwich which is composed of the very small, 6 amino acid, α-Helix
226 II and loops. In the canonical TPM domain two and three longer α-helices are present on
227 each side of the β-sheet.
228 Of the six structures deposited in the Protein Data Bank, 3 appear as metal binding
229 proteins Rhom172_1776, AtTLP18.3, and BA42. A cofactor-binding site is identifiable at
230 one of the N-terminus loops of the LMTP1 protein between β-strands A and α-helices I.
231 Notably, this does not correspond to the proposed Ca^{2+}-binding site in AtTLP18.3 (Wu et
232 al., 2011) or the Ca^{2+}/ Mg^{2+} sites in BA42 (Aran et al., 2014; Pellizza et al., 2016), but is
233 conserved as a Mg^{2+} binding site, with a conserved coordination sphere for the metal, in
234 Rhom172_1776. Unfortunately, Rhom172_1776 has been deposited without being
235 published thus far, making it difficult to infer a function uniquely based on this structure.
236 The binding site in LMTP1 is occupied by a divalent hexa-coordinated metal coordinated
237 by waters, side chains of protein residues Asp97, Glu107, and the carbonyl group of
238 Leu102 (Asp44, Leu49, and Glu54 in the recombinant protein sequence) which are all
239 conserved in the *Cyanobacteriota* and Arabidopsis homologues, but not in the algal
240 paralogue TLP26 nor in TLP18.3 (see Figure 3 inset). The crystal also shows that the
241 cysteine pair at the C-terminus of the protein is oxidized, forming an intra-molecular
242 disulfide bridge, which could be important for the function and stability of the protein.
243 The modelled divalent ion in the LMTP1 structure is Ca^{2+}, but as we suspected this
244 may be a crystallization artefact, to determine what divalent metal really binds to
245 recombinant LMTP1, and to determine if the same metal could also bind to TLP26, we
246 used nano-differential scanning fluorimetry (nanoDSF) with an array of different divalent
247 metals in a 1:5 (protein:metal) ratio. For LMTP1, Cu^{2+} decreased the thermal stability of
248 the protein, whereas Ca^{2+} and especially Mn^{2+} significantly increased the thermal stability
249 of LMTP1 (Figure 4a); for TLP26, no tested divalent metal caused a significant shift in the

250 thermal stability of the protein (Figure 4b). Based on the coordination spheres of Cu^{2+},
251 Ca^{2+}, and Mn^{2+}, Mn^{2+} typically displays a hexa-coordination, in agreement with the cofactor
252 binding site of the LMTP1 structure; Finally, Alphafold3 modelling of LMTP1 with a Mn^{2+}
253 added as a cofactor result in an identical prediction for binding site as found in our
254 structure, coordinated by the same residues (Supplemental Figure 1c). As for the other
255 divalent metals that trigger thermal stability shifts on LMTP1, Ca^{2+} should rather be
256 octahedrally coordinated, thus not fitting into the cofactor binding site, and even though
257 Cu^{2+} can be hexa-coordinated, when modelling the interaction via Alphafold3 the metal is
258 predicted to bind to different protein residues (Supplemental Figure 1d), thus it is unlikely
259 that Cu^{2+} could be the cofactor of LMTP1.
260 As we observed that the recombinant LMTP1 cysteines enable the formation of
261 intramolecular disulfide bridges, we investigated the effect of the redox status of these
262 residues on the protein conformation. We incubated the protein under oxidizing (+ H_2O_2)
263 or reducing (+ TCEP) conditions, and in the absence or presence of selected divalent
264 metals. Under reducing conditions, the thermal stability of LMTP1 increases, even without
265 adding any metals, while it seems to remain unchanged for oxidizing conditions; for all
266 tested conditions, incubation with manganese significantly increased the thermal stability
267 of the protein vs. the condition with no metals added (Figure 4c).
268
269 *LMTP1 and TLP26 exhibit very low phosphatase activity*
270 The TPM-domain family of proteins is also annotated as "Thylakoid acidic phosphatase"
271 (TAP) domain in *Arabidopsis thaliana* (TPM domain (IPR007621) - InterPro entry -
272 InterPro), based on the activity of one member of this family of proteins, TLP18.3 (Wu et
273 al., 2011). Based on this annotation, LMTP1 was proposed as another potential functional
274 partner required for the phosphatase action of a luminal complex regulated by CYP38
275 (Hao et al., 2021). Here, we have tested the phosphatase activity of our recombinant
276 LMTP1 and TLP26 against the substrate *p*NPP.
277 When incubating the recombinant protein with different concentrations of substrate
278 (with or without the addition of 2 molar equivalents of Mn^{2+} for LMTP1) we observed a very
279 low activity, from 0.2 to 0.4 nmol phosphate·mg^{-1}·min^{-1}, which is in line with the activity
280 reported for other TPM domain proteins (Wu et al., 2011; Pellizza et al., 2016; Cerutti et
281 al., 2017). As a comparison, 1 unit of the commercial Alkaline Phosphatase showed the
282 expected activity of 1 μmol of substrate per minute (1000 nmol phosphate·mg^{-1}·min^{-1}).
283 If this very low phosphatase activity is specific to TPM-domain proteins it follows that a
284 conserved set of amino acids should be identifiable within the putative TAP domain. When
285 aligning the sequences of different homologues of LMTP1 from different species with

286 CrTLP26 and CrTLP18.3 we did not identify a clearly conserved region between the
287 different proteins (Supplemental Figure 2).
288
289 *LMTP1 is the paralogue conserved in all oxygenic phototrophs and TLP26 is only present*
290 *in a cluster of primary endosymbionts*
291 LMTP1 and TLP26 have different metal-binding affinities and structural differences,
292 namely the presence or absence of C-terminus transmembrane helices. We then
293 hypothesized that the two paralogues could be two distinct proteins with a common
294 ancestor that have evolved to play different roles during light acclimation in phototrophic
295 organisms. To this end, we compared the mature sequences (i.e., without transit peptides
296 as predicted by TargetP 2.0 (Almagro Armenteros et al., 2019)) of both our *C. reinhardtii*
297 paralogues with the LMTP1 homologues from *A. thaliana* and Synechocystis, as well as
298 the sequence of another TPM-domain protein from *C. reinhardtii*, TLP18.3 (Supplemental
299 Figure 2).
300 Based on multiple sequence alignments, CrLMTP1 is the homologous protein that
301 has the strongest sequence similarity with those of both Synechocystis and Arabidopsis.
302 In all these proteins, we have identified that the manganese-binding site is conserved, as
303 well as a tyrosine residue that has been shown to be phosphorylated *in vivo* in A*. thaliana*
304 (Gollan et al., 2021). CrTLP26 and TLP18.3 do not share either the conserved metal-
305 binding site, or the phosphorylated residue, thus LMTP1 is likely the conserved paralogue
306 throughout oxygenic phototrophs.
307 To strengthen this hypothesis, we built phylogenetic trees using a maximum
308 likelihood method for LMTP1 and TLP26 (Figure 6, Supplemental Figure 3). The trees
309 were drawn based on the protein family PTHR35514 (Thylakoid_lumenal_15kDa-like),
310 which is conserved in photosynthetic organisms only, including *Cyanobacteriota*. Given
311 the evolutionary history of photosynthesis (Hohmann-Marriott and Blankenship, 2011;
312 Cardona, 2019), it is very likely that this family of proteins in photosynthetic eukaryotes
313 emerged from an endosymbiotic *Cyanobacteriota* ancestor, followed by a duplication
314 event in the last common ancestor to all *Streptophyta* (including green algae, mosses, and
315 land plants). *C. reinhardtii* harbors two paralogous proteins: **(i)** LMTP1 (encoded by
316 Cre15.g636050 and previously annotated as CPLD31) that clusters with proteins of land
317 plants and that is conserved in all oxygenic photosynthetic organisms, and **(ii)** TLP26
318 (encoded by Cre03.g154600 and previously annotated as TLP15.2) that clusters with
319 membrane-docked proteins conserved only in primary endosymbionts. The longer
320 external branches, indicative of higher evolutionary rates, support the neofunctionalization

321 of TLP26, that we predict to have arisen after the duplication event and primary
322 endosymbiosis, while LMTP1 function remained similar to that of the prokaryotic ancestor.
323
324
325 ## Discussion
326
327 The TPM-domain superfamily of proteins (InterPro entry IPR007621) is widely conserved
328 across *Bacteriota* and is limited to invertebrates and phototrophs amongst *Eukaryota*. The
329 given name "TPM" is based on the first three proteins studied from this family: TLP18.3
330 from *A. thaliana*, Psb32 from *Synechocystis sp. PCC6803*, and MOLO-1 from *C. elegans*
331 (Pellizza et al., 2016). Despite the low conservation in primary sequences of TPM domain
332 proteins, they can be identified by their conserved and unique secondary structure,
333 composed of a central hydrophobic β-sheet, made of four β-strands, flanked by four
334 amphiphilic α-helices (Cerutti et al., 2017). While the function and role of most TPM-
335 domain proteins is unknown, as well as the relationship between protein structure and
336 physiological role (Pellizza et al., 2016), some proteins of this family have been proposed
337 to play a role in PSII repair and acclimation to high light (Sirpiö et al., 2007; Wegener et
338 al., 2011).
339 The uncharacterized family of TPM-domain proteins, PTHR35514
340 (Thylakoid_lumenal_15kDa-like) were included in the GreenCut library published with the
341 Chlamydomonas genome, highlighting their conservation (Merchant et al., 2007; Chazaux
342 et al., 2020). Members of the PTHR35514 family of proteins have been detected as
343 peptides in proteomics studies in *C. reinhardtii (Colina et al., 2020)*, *A. thaliana* (Gollan et
344 al., 2021), and *Cyanobacteriota* (Dahlgren et al., 2021). In *A. thaliana,* the AT5G52970
345 protein was proposed to be a constituent of the soluble fraction of the thylakoid lumen
346 (Gollan et al., 2021), and in *Cyanobacteriota* Sll1071 peptides form part of the interactome
347 of the PsbU subunit of PSII, equally in the thylakoid lumen (Dahlgren et al., 2021). The
348 green algae *C. reinhardtii* encodes two paralogues of proteins from these family, LMTP1
349 (encoded by Cre15.g636050) and TLP26 (encoded by Cre03.g154600). Based on TargetP
350 2.0 predictions (Almagro Armenteros et al., 2019), both proteins are addressed to the
351 thylakoid lumen, and according to their predicted secondary structure via Alphafold3
352 (Hallgren et al., 2022) LMTP1 is a soluble protein, while TLP26 is membrane-docked via
353 three C-terminus transmembrane alpha-helices (Supplemental Figure 1a).
354 We generated knock-out mutants of *LMTP1* and *TLP26* in *C. reinhardtii* via
355 CRISPR/Cas9, confirmed by PCR (Figure 1b) and immunoblot analysis (Figure 1d). We
356 have confirmed the secondary structure predictions for both proteins (Supplemental Figure

357 1a), as TLP26 is detected in thylakoid membrane protein extracts, unlike for LMTP1. Under
358 photoautotrophic conditions at non-saturating light intensities, the mutants divide at WT
359 rates and have functional PSII centers, as assessed by F_V/F_M levels (Figure 2b). This is
360 not unexpected, as *tlp18.3*, involved in photosynthetic acclimation, has normal growth
361 under standard conditions (Sirpiö et al., 2007). During the shift from photomixotrophy to
362 photoautotrophy the accumulation of LMTP1 increases in WT *C. reinhardtii* cells, and upon
363 shift to high light illumination both LMTP1 and TLP26 protein contents increase (Figure
364 2a). Additionally, when filtering data from circadian regulation of *C. reinhardtii* genes
365 (Zones et al., 2015) we can observe that *LMTP1* mRNA transcript abundance follows a
366 circadian pattern, like *TLP18.3*, whereas *TLP26* seems to increase on the onset of
367 illumination and immediately decrease for the remaining day (Figure 2c); the behavior of
368 *TLP26* resembles *VTC2*, a gene that encodes GDP-L-galactose phosphorylase, a key
369 enzyme in the biosynthesis of Vitamin C in *C. reinhardtii* (Vidal-Meireles et al., 2017). Like
370 TLP18.3 (Sirpiö et al., 2007), LMTP1 may play a role in PSII turnover during phototrophic
371 acclimation, while TLP26 may play a role during the dark-to-light transition, ensuring the
372 fitness of the cells while the photosynthetic apparatus is not yet fully active.
373 We showed the presence of a TPM-fold in LMTP1 by resolving its crystal structure
374 (Figure 3), and found a novel metal binding site, coordinated by Asp97, Glu107, and
375 Leu102 that are conserved in LMTP1 homologues from different species (Asp44, Leu49,
376 and Glu54 in the recombinant protein sequence). However, in TLP26 and TLP18.3 Glu107
377 is replaced by an arginine. Of the few TPM-domain containing protein crystal structures
378 available in the PDB, only one shares the same coordination sphere as observed for
379 LMTP1, but this structure is deposited as a magnesium binding protein and remains
380 unpublished. Based on fluorescence emission thermal denaturation assays (Figure 4a),
381 the most likely metal that occupies the cofactor site at LMTP1 is Mn^{2+}; this is also a novel
382 finding within the TPM-domain family of proteins, as Mg^{2+} and Ca^{2+} have been the only
383 divalent metals reported as cofactors of BA42 and TLP18.3 (Wu et al., 2011; Pellizza et
384 al., 2016). Interestingly, Mn^{2+} was suggested to play a role in the activity of BA41, but no
385 direct proof of protein binding was shown in that work (Cerutti et al., 2017). Mn^{2+} typically
386 binds to hard atoms such as oxygen (O) and nitrogen (N), with a generally hexa-
387 coordinated geometry, as observed in our crystal structure (Figure 3). The amino acids
388 involved in this binding mainly include aspartic acid (Asp) and glutamic acid (Glu), through
389 the oxygen atoms of their side chains (Khrustaleva, 2014). These observations further
390 support that Mn^{2+} is the cofactor of LMTP1. The specificity of the observed interaction and
391 the dissociation constant between metal and protein remain to be determined. It is worth
392 commenting that Cu^{2+} impacts the thermal stability of LMTP1, which we attribute to a likely

393 oxidizing effect of Cu^{2+} on the protein (McCann and Stahl, 2015). We have not yet resolved
394 the structure of TLP26, but the change of one of the key aminoacids at the metal-binding
395 site (E54R) and the absence of changes to thermal stability upon incubation with different
396 divalent metals (Figure 4b) suggest that the metal-binding site of LMTP1 is not conserved
397 in TLP26.

398 The crystal structure of LMTP1 also revealed that the cysteines at the C-terminus
399 of the protein form disulfide bridges. As LMTP1 expression responds to high light (Figure
400 2a) and it has been proposed as a thioredoxin target (Pérez-Pérez et al., 2017), we
401 evaluated the effect of redox changes on the thermal stability of the protein (Figure 4c).
402 Under reducing conditions, the thermal stability of LMTP1 was the highest, increasing in
403 the presence of Mn^{2+}. This result is not surprising, as thylakoid lumen proteins are known
404 to be more stable in their reduced inactive form, being transported across the thylakoid
405 membrane in this state and only getting oxidized when triggered by rapid changes to ROS
406 content or acidification (Hoh et al., 2024). The change in the redox status of the cysteines
407 can occur upon interaction with thioredoxins, probably at long distance via signal
408 transduction from the stroma (Hoh et al., 2024). In *A. thaliana*, nearly half of all lumenal
409 proteins have been identified as targets of thioredoxin in *in vitro* studies; this contrasts with
410 the chloroplast stroma, where only about 2% of the proteins are regulated in this manner
411 (Lindahl and Kieselbach, 2009; Hall et al., 2010). Examples of redox regulation in the
412 lumen include several proteins that are essential for light acclimation, such as STN7,
413 FKBP13, and VDE (Gopalan et al., 2004; Lemeille et al., 2009; Lu et al., 2015; Wu et al.,
414 2021). Besides thioredoxin regulation, proteins also respond to lumen acidification upon
415 high light exposure. The changes in the lumenal pH trigger shifts in the protein redox
416 potentials, and also impact the protonation of different protein residues, which promote
417 conformational changes that shift the accessibility of these residues in the protein,
418 including cysteine pairs (Hoh et al., 2024).

419 TLP18.3, BA42, and Rv2345, three TPM-domain proteins, have been proposed to
420 function as phosphatases, albeit with very low activities (Wu et al., 2011; Sinha et al., 2015;
421 Pellizza et al., 2016); this lead to an annotation of “Thylakoid Acidic Phosphatase” (TAP)
422 within the TPM domain (Supplemental Figure 2). This is connected to *A. thaliana* CYP38
423 involvement in PSII core and antenna protein de-phosphorylation, a function that was
424 outsourced to interacting proteins and speculated as LMTP1 or TLP18.3, based on *in vitro*
425 pull-down assays (Sirpiö et al., 2008; Hao et al., 2021). To evaluate if LMTP1 and TLP26
426 are acidic phosphatases, we used the general phosphorylated substrate *p*NPP, which
427 when incubated under acidic conditions showed 5000 times less activity for our
428 recombinant proteins than the positive control used (Alkaline Phosphatase). The rate of

429 *p*NPP hydrolysis was in the same range (0.2-0.4 nmol phosphate·mg^{-1}·min^{-1}) as that
430 observed for the other proteins of the TPM-domain superfamily (Wu et al., 2011; Sinha et
431 al., 2015; Pellizza et al., 2016), suggesting that the TPM-fold may be responsible for the
432 conserved, yet exceptionally feeble, phosphatase activity of these proteins. That addition
433 of Mn^{2+} to LMTP1 does not have an effect on its activity further supports that TPM-domain
434 proteins are constitutively able to hydrolyze phosphate residues, even without the
435 presence of a cofactor. When comparing the sequence alignment of different homologues
436 of LMTP1 with TLP26 and TLP18.3, we were unable to identify conserved regions that
437 could support the presence of a common domain responsible for the phosphatase activity
438 of these proteins (Supplemental Figure 2). A second, equally low, activity as hydrolases of
439 di- and triphosphate nucleotides has also been shown for Rv2345 and BA41, with an
440 enhanced activity after Mn^{2+} incubation for BA41 (Sinha et al., 2015; Cerutti et al., 2017).
441 The physiological relevance of this very low phosphatase activity remains yet to be
442 determined.
443 To understand the evolutionary history of LMTP1 and TLP26, and to correctly
444 annotate them, we have compared them to other members of its protein family
445 (PTHR35514 – Thylakoid_lumenal_15kDa-like) from various prokaryotic and eukaryotic
446 oxygenic phototrophs and built both unrooted (Figure 6) and rooted (Supplemental Figure
447 3) phylogenetic trees. When unrooted (Figure 6), we have two clear groups of proteins,
448 one containing TLP26 from *C. reinhardtii* and homologues from primary *Chlorophyte*
449 endosymbionts, and another containing LMTP1 from *C. reinhardtii*, the cyanobacterial
450 homologue Sll1071, and the *A. thaliana* homologue AT5G52970. This division is coherent
451 with the sequence alignment of the different homologues, because TLP26 is the most
452 divergent (Supplemental Figure 2). Key residues, such as the metal-binding site identified
453 in this manuscript and an *in vivo* phosphorylatable Tyr residue, identified via proteomics
454 studies in *A. thaliana* (Gollan et al., 2021), are highlighted in Figure 3 and Supplemental
455 Figure S2.
456 We also noted that the distance between cysteines appears to depend on the
457 presence or absence of the C-terminus transmembrane helices: for CrLMTP1 and
458 AtLMTP1 (soluble proteins), the distance between these aminoacids is longer than for
459 CrTLP26 and Sll1071 (membrane-docked proteins). As there are no cysteines in TLP18.3,
460 these are clearly not a requirement for the formation of the TPM-domain and rather may
461 play a specific role on LMTP1 and TLP26 regulation. Additionally, the transmembrane
462 domains of both CrTLP26 and Sll1071 share some degree of similarity, and CrLMTP1,
463 although it is a soluble protein, has some amino acids at its C-terminus that align to this
464 transmembrane region, hinting that it was originally a membrane-docked protein that has

465 eventually evolved to be fully soluble. Data also suggest that both proteins evolved from a
466 common, cyanobacterial, ancestor, which was duplicated in the early endosymbiotic
467 species, followed by the specialization of each paralogue. Why plants and algal secondary
468 plastid endosymbionts do not have TLP26 is intriguing and may hold the key to
469 understanding the functionality of these paralogues.
470 When rooting the trees (Supplemental Figure 3) using a homologue of Sll1071 as
471 the last common ancestor of the PTHR35514 family of proteins, we observe the same
472 branch distribution of the homologues, further strengthening the hypothesis that LMTP1 is
473 the conserved homologue in all oxygenic photosynthetic organisms.
474 Finally, the previous annotations of LMTP1 and TLP26 from *C. reinhardtii* are
475 incorrect. LMTP1, encoded by Cre15.g636050 was previously annotated as "Conserved
476 in the Plant Lineage and Diatoms 31" (CPLD31), which excludes the homologues present
477 in *Cyanobacteriota*; TLP26, encoded by Cre03.g154600, was annotated as "Thylakoid
478 Lumenal 15.0 KDa Protein 2, Chloroplastic" (TLP15.2), which did not match its actual
479 molecular weight – 26.3 kDa.
480
481 We therefore reannotate the TPM-domain homologue encoded by Cre15.g636050
482 **L**umenal **M**n-binding **T**PM-domain **P**rotein **1** (LMTP1); all other homologues throughout
483 the green lineage and *Cyanobacteriota*, such as Sll1071 and AT5G53970, share this
484 conserved manganese-binding site. The other TPM-domain protein, encoded by
485 Cre03.g154600 (and all the homologues in the Chlorophyta clade), with a yet unknown
486 structure and function, should be annotated as **T**hylakoid **L**umenal **P**rotein **26** kDa
487 (TLP26).
488
489
490 ## Materials and Methods
491
492 <u>*Cell culture*</u>
493 The wild-type strain (T222 mt+) used in this study is a progeny of 137c backcrosses
494 (Bujaldon et al., 2017). Maintained cultures were always cultivated at 20 µmol photons·m^{-}
495 ^{2}·s^{-1} in TAP + 2 % agar media plates. For experimental setups, liquid cell cultures were
496 grown in Tris-Acetate-Phosphate (TAP) medium at 25°C under ambient air at continuous
497 25 µmol photons·m^{-2}·s^{-1} illumination in incubation shakers (photomixotrophic conditions),
498 and when stated, shifted to photoautotrophic conditions by centrifugation and
499 resuspension in minimal (MIN) media under ambient air at the described light intensities.

500 Standard recipes for media preparation were used as in (Harris, 1989). Experiments were
501 performed using batch cultures in 100- or 500-ml Erlenmeyer flasks. Cell division rates
502 were estimated via absorption changes at 720 nm.
503
504 *Generation of C. reinhardtii CRISPR/Cas9 mutants*
505 The transformation was performed based on (Yu et al., 2017; Kelterborn et al., 2022), with
506 some modifications. Briefly, specific gRNAs and Alt-R™ S.p. Cas9 Nuclease V3 were
507 ordered from IDT-DNA and used to assemble *in vitro* RNP particles. *C. reinhardtii* wild-
508 type cells were harvested at early exponential stage ($2x10^6$ cells·ml^{-1}) via centrifugation
509 (1600 g, 5 min, RT), and re-suspended in "MAX Efficiency™ Transformation Reagent for
510 Algae" (Thermo Fisher Scientific), supplemented with 20 % sucrose, to a final
511 concentration of $2x10^8$ cells·ml^{-1}. A heat-shock (40 ºC, 30 min, 450 rpm shaking) was then
512 applied to the cells, followed by a 20-min recovery at RT, before 120 µl of cells were added
513 to a pre-cooled 2-mm gap electroporation cuvette together with 15 µl of RNP particles and
514 1 µg of paromomycin-resistance plasmid for electroporation (600 V, 50 µF, infinite external
515 resistance). Cells were allowed to recover overnight in TAP medium supplemented with
516 20 % sucrose and 1 mg·l^{-1} Vitamin B12 at 33 ºC in the dark before being plated in TAP +
517 2 % agar + 10 mg·l^{-1} paromomycin and incubated under 20 µmol photons·m^{-2}·s^{-1}
518 illumination until colonies could be picked.
519
520 *DNA isolation and PCR*
521 Total genomic DNA and PCR were done using the "Phire Plant Direct PCR Master Mix" kit
522 (Thermo Fisher Scientific) according to the manufacturer's instructions. Briefly, a small
523 amount of cells was solubilized with 20 µl of "Dilution buffer" (included in the PCR kit) via
524 agitation, before centrifugation (4000 g, 10 min, RT) to obtain the DNA in the soluble
525 fraction. The PCR master mix was prepared by mixing 5 µl of 2X reagent with 3 µl of 3 M
526 betaine, 1 µl of each primer, and 1 µl of DNA template (or ddH_2O as a negative control),
527 and amplification was done during 35 cycles. PCR products were loaded on a 3 % TAE-
528 agarose gel and the DNA was stained for visualization with ClearSight (Euromedex). The
529 primers used to amplify the *lmtp1* gene are 5'-TTGTCAACATGCAGAGCCTC-3' and 5'-
530 TAGTTGCAGCCAGTAGTCGT-3' (corresponding to an WT-sized amplicon of 249 bp) and
531 for the *tlp26* gene are 5'- ATGCAAGTTTACGGGAATGCA-3' and 5'-
532 GATGCCAGTACACCACGTCTT-3' (corresponding to an WT-sized amplicon of 748 bp).
533
534 *Protein isolation*

535 Protein extraction was based on (Riché et al., 2024) with minor modifications. Briefly, 5-ml
536 of culture was collected at each time-point, centrifuged (20800g, 1 min, RT), and the pellets
537 were frozen in liquid N_2 before being re-suspended in 350 µl of lysis buffer (50mM Tris pH
538 6.8, 2% SDS, 1 mM DTT, 1 mM PMSF, 1X cOmplete protease inhibitor without EDTA –
539 Sigma Aldrich) and incubated at 37 ºC for 30 min with strong agitation. Chlorophyll content
540 was determined via methanol extraction (Porra et al., 1989).
541
542 *Thylakoid isolation*
543 Thylakoid extraction was done according to the standard method (Chua and Bennoun,
544 1975) and the thylakoids were resuspended in a final 5 mM HEPES/KOH pH 7.5 at 1
545 mg/mL chlorophyll for subsequent immunoblot analysis.
546
547 *Immunoblot analysis*
548 Western blot analysis was performed as in (Chazaux et al., 2020) with minor modifications.
549 Briefly, proteins were separated under denaturing conditions on 15% SDS-PAGE gels
550 supplemented with 4 M Urea. Samples were loaded based on chlorophyll content (100 %
551 equals 1 µg protein). Proteins were transferred onto nitrocellulose membranes (BioTrace
552 NT, Pall Corporation) using liquid transfer. Primary LMTP1 and TLP26 antibodies were
553 generated in rabbit against the recombinant protein (ProteoGenix) and used at a 1:5000
554 ratio; primary Atpβ antibody was a kind gift from S. Bujaldon and used at a 1:100000 ratio.
555 Secondary antibodies used were always HRP-conjugated anti-rabbit (Invitrogen). HRP-
556 peroxidase chemiluminescent substrate (SuperSignal™ West Pico PLUS, Thermo Fisher
557 Scientific) was used to reveal the antibody signal, using a GBOX imaging system
558 (Syngene).
559
560 *Chlorophyll a fluorescence analysis*
561 Chlorophyll *a* fluorescence kinetics were determined using the Joliot-type
562 Spectrophotometer (JTS-Biologic). Dark-adapted cells were subjected to a saturating
563 pulse (8 000 µmol photons$\cdot m^{-2} \cdot s^{-1}$) to measure F_V/F_M.
564
565 *Recombinant protein production*
566 The protocol for production of recombinant proteins was based on (Chazaux et al., 2020).
567 The synthetic DNA sequences of *C. reinhardtii lmtp1* (corresponding to the residues R77
568 to K246 of Cre15.g636050) and *tlp26* (corresponding to the residues A82 to V226 of
569 Cre03.g154600) genes, flanked by complementary *BsaI* restriction sites sequences, were

570 ordered from Twist Bioscience and sub-cloned into the plasmid pNIC28-Bsa4
571 (Addgene#26103) using GoldenGate cloning technique. The pNIC28-Bsa4 vector
572 contains a 6×His-tag and a TEV protease-cleavage site followed by the suicide
573 gene *sacB* (flanked by *BsaI* restriction sites), which is replaced by our synthetic gene
574 sequences. 20 fmol of vector was used with 20 fmol synthetic DNA for three successive
575 rounds of digestion (*BsaI*, 37°C, 10 min) and ligation (T4 DNA ligase, 16°C, 10 min) in the
576 same mix. TOP10 *E. coli* cells (NEB) were then transformed with the ligation products for
577 vector amplification, screening and sequencing. 50 ng of vector were then used to
578 transform chemically competent *E. coli* BL21(DE3) cells (Invitrogen) for protein
579 expression.
580 Bacterial cells were cultured at 37 °C in Luria Broth (Lennox) supplemented with
581 50 μg·ml^{-1} of kanamycin. Expression was induced once cells reach an OD_{600} of 0.6-0.8 by
582 addition of 500 μM IPTG, and the cultures were left overnight at 17 °C. Cells were collected
583 by centrifugation and re-suspended in lysis buffer (50 mM Sodium-Phosphate buffer,
584 300 mM NaCl, 10 mM Imidazole, pH 8.0) supplemented with protease inhibitor cocktail
585 (Sigma-Aldrich) and DNase. Lysis buffer was used in the ratio of 1.5 ml buffer per 1 g of
586 wet cell pellet. Re-suspended pellets were stored at -80 °C.
587 Cells were disrupted twice by French Press at 1000 psi and clarified by
588 centrifugation at 40000 x *g* for 45 min. Purification of the His-tagged proteins was
589 performed in two steps, using Ni-charged HisTrap HP (Cytiva) and HiLoad 16/60 Superdex
590 200 pg columns (Cytiva) on an ÄKTA Pure FPLC protein purification system (Cytiva); the
591 columns were pre-equilibrated with IMAC buffer (50 mM Sodium-Phosphate, 300 mM
592 NaCl, 10 mM Imidazole, pH 8.0) and gel filtration buffer (20 mM MES, 150 mM NaCl, pH
593 6.5), respectively. The 0.45 μM filtered lysates were loaded onto the HisTrap HP
594 column and washed with IMAC buffer. Bound protein was eluted with IMAC buffer
595 containing 250 mM imidazole and cleavage of the 6xHis-tag was done overnight at 4 ºC,
596 using recombinant TEV protease at a 1:20 (TEV:target protein) ratio by dialysis
597 against IMAC buffer without imidazole. Cleaved protein was separated from the tag and
598 the TEV protease by a second run on Histrap HP column and loaded onto the pre-
599 equilibrated gel filtration column. Fractions containing the target proteins were pooled and
600 concentrated using a VIVASPIN centrifugal filter device with a cut-off size of 10 kDa.
601 Protein purity was confirmed by SDS–polyacrylamide gel electrophoresis and protein
602 samples were flash frozen in liquid nitrogen and stored at -80 °C.
603
604 <u>*Crystallization, data collection, structure determination and validation*</u>

605 Native crystals were obtained by the “sitting drop vapour” diffusion method in a 96-well
606 plate. 0.5 µl of protein solution (at a concentration of 6.3 mg·ml^{-1}) in gel filtration buffer
607 (20 mM MES, 150 mM NaCl, pH 6.5) was mixed with 0.5 µl of “well solution”, consisting of
608 0.2 M $CaCl_2$, 0.1 M HEPES/KOH pH7.0 and 20% (w/v) PEG 6000. The plate was
609 incubated at 20 °C and crystals were obtained after 12-14 days. Crystals were quickly
610 transferred to cryogenic solution containing well solution with 20 % glycerol, and flash
611 frozen in liquid nitrogen.
612 Native data were collected to 1.6 Å on beamline BM07 at the ESRF Synchrotron
613 facility (France). Data integration and scaling were performed with the EDNA auto-
614 processing pipeline on the beamline. The structure was solved by the MrBUMP (Keegan
615 and Winn, 2007) in the CCP4 suite (Collaborative Computational Project, Number 4,
616 1994).
617 Models were generated by successive rounds of building and refinement with Coot
618 and Refmac5, respectively (Murshudov et al., 1999; Emsley and Cowtan, 2004). Structure
619 validations were performed using the Molprobity server
620 (http://molprobity.biochem.duke.edu/) and Procheck from the CCP4 suite (Collaborative
621 Computational Project, Number 4, 1994). Coordinates and structure factors have been
622 deposited in the Protein Data Bank under PDB ID 9H70.
623
624 *Thermal unfolding experiments via* nano-differential scanning fluorimetry *(nanoDSF)*
625 For thermal unfolding experiments, proteins were diluted to a final concentration of 10 µM
626 and incubated with 5 molar excess of each divalent metal. In redox experiments (Figure
627 4c), proteins were first incubated for 4 h at 25 ºC with freshly prepared 2 mM H_2O_2 or 2
628 mM tris(2-carboxyethyl)phosphine (TCEP). For each condition, 10 µl of sample per
629 capillary were required for one thermal unfolding profile. The samples were loaded into
630 Prometheus capillaries (NanoTemper Technologies) and experiments were carried out
631 using the Prometheus NT.48. The temperature ramp was set to an increase of 1 °C/min in
632 a range from 20 °C to 90 °C. Protein unfolding was measured by detecting the
633 temperature-dependent change in tryptophan fluorescence at emission wavelengths of
634 330 and 350 nm. For calculation of Melting Temperature (Tm), the first derivative data of
635 the F_{350}/F_{330} fluorescence ratio unfolding curves were used.
636
637 *Phosphatase activity assays*
638 The hydrolysis rate of *p*-nitrophenyl phosphate (*p*NPP, NEB) was determined based on
639 (Wu et al., 2011). Briefly, 10 µg (about 0.6 nmol) of recombinant protein were mixed with
640 different concentrations of substrate, and the volume was completed with recombinant

641 protein buffer (20 mM MES, 150 mM NaCl pH 6.5) up to 100 µl; when applicable, 2 molar
642 excess of Mn^{2+} were added to the reaction. As a positive control, 1 U of Alkaline
643 phosphatase was used instead of recombinant protein. The samples were incubated at
644 RT for 1 h before quenching the reaction with 100 µl of 1 N NaOH and measuring
645 absorbance at 405 nm.
646
647 *Phylogenetic analysis*
648 A phylogenetic tree of the thylakoid acid phosphatase family was built from sequences of
649 the PANTHER entry PTHR35514 / Thylakoid_lumenal_15kDa-like, some of which are also
650 classified in the InterPro entry IPR007621 / TPM_dom family. A set of homologous amino-
651 acid sequences representing the major taxa were selected in the dbUniProtKB reference
652 proteomes and Swiss-Prot databases, including eukaryotic lineages from the
653 *Streptophyta*, *Chlorophyta*, *Rhodophyta*, and the *Stramenopiles-Alveolata-Rhizaria* group.
654 A multiple sequence alignment was performed with MAFFT v7.49 (Katoh and Standley,
655 2013) using the L-INS-i strategy, and filtered for saturation with BMGE v1.12 (Criscuolo
656 and Gribaldo, 2010) using the BLOSUM30 matrix and removing sites with > 50% gaps, to
657 get a final alignment containing 189 sites and 51 sequences. The tree was built using the
658 Maximum-Likelihood (ML) algorithm with IQ-TREE (Minh et al., 2020) and the
659 Q.pfam+I+R4 substitution model selected by ModelFinder (Kalyaanamoorthy et al., 2017)
660 with the Bayesian Information Criterion (BIC) (Supplementary Figure S3). The statistical
661 support of the branches was estimated using a (UFBoot) approximation (Hoang et al.,
662 2018) implemented in IQ-TREE with 1000 replicates. A second tree was built from a
663 reduced dataset of 36 sequences aligned and trimmed to get an alignment of 215 sites,
664 and representing *Embryophyta*, *Chlorophyta* and *Cyanobacteriota* only (Figure 6).
665
666 *Statistical analysis*
667 When applicable, data is presented as Average ± Standard deviation. Statistical
668 significance was determined using one-way ANOVA followed by Dunnett multiple
669 comparison posttests (GraphPad Prism 9.3.0; GraphPad Software). Changes were
670 considered statistically significant at $p < 0.05$ and presented as: $p < 0.05$, 1 symbol; $p <$
671 0.01, 2 symbols; $p < 0.001$, 3 symbols.
672
673
674 **Author contributions**
675

AV-M, MS, XJ designed the research; AV-M, SM, YH, CM, MS, XJ performed research; AV-M, SM, CM, MS, JA, XJ analyzed data; AV-M, CM, MS, XJ wrote the paper.

Acknowledgements

We thank Géraldine Brandelet and Clara Amselem of the ProteinTec platform of the BIAM for the help with protein production and crystallization. We also warmly thank Stefania Viola, Bernard Genty, Corinne Cassier-Chauvat, Stefano Caffarri, Franck Chauvat, Pathomchai Dindaeng, and Chloé Maurin for helpful discussions and their involvement in this project.
We are grateful to the INRAE MIGALE bioinformatics platform (https://migale.inrae.fr/) for providing computational resources. This work was supported by a grant from the French Agence National de la Recherche (RevelOrg: ANR-20-CE20-0006).

References

Abramson J, Adler J, Dunger J, Evans R, Green T, Pritzel A, Ronneberger O, Willmore L, Ballard AJ, Bambrick J, et al (2024) Accurate structure prediction of biomolecular interactions with AlphaFold 3. Nature **630**: 493–500

Almagro Armenteros JJ, Salvatore M, Emanuelsson O, Winther O, Von Heijne G, Elofsson A, Nielsen H (2019) Detecting sequence signals in targeting peptides using deep learning. Life Sci Alliance **2**: e201900429

Aran M, Smal C, Pellizza L, Gallo M, Otero LH, Klinke S, Goldbaum FA, Ithurralde ER, Bercovich A, Mac Cormack WP, et al (2014) Solution and crystal structure of BA42, a protein from the Antarctic bacterium *B izionia argentinensis* comprised of a stand-alone TPM domain: Structure of BA42 from *Bizionia argentinensis*. Proteins Struct Funct Bioinforma **82**: 3062–3078

Baena–González E, Aro E (2002) Biogenesis, assembly and turnover of photosystem II units. Philos Trans R Soc Lond B Biol Sci **357**: 1451–1460

Beck C, Knoop H, Steuer R (2018) Modules of co-occurrence in the cyanobacterial pan-genome reveal functional associations between groups of ortholog genes. PLoS Genet **14**: e1007239

710 **Bujaldon S, Kodama N, Rappaport F, Subramanyam R, De Vitry C, Takahashi Y,**
711 **Wollman F-A** (2017) Functional Accumulation of Antenna Proteins in Chlorophyll
712 b-Less Mutants of Chlamydomonas reinhardtii. Mol Plant **10**: 115–130
713 **Cardona T** (2019) Thinking twice about the evolution of photosynthesis. Open Biol **9**:
714 180246
715 **Cerutti ML, Otero LH, Smal C, Pellizza L, Goldbaum FA, Klinke S, Aran M** (2017)
716 Structural and functional characterization of a cold adapted TPM-domain with
717 ATPase/ADPase activity. J Struct Biol **197**: 201–209
718 **Chazaux M, Caffarri S, Da Graça J, Cuiné S, Floriani M, Brzezowski P, Peltier G,**
719 **Genty B, Alric J, Johnson X** (2020) ACCLIMATION OF PHOTOSYNTHESIS TO
720 THE ENVIRONMENT 1 regulates Photosystem II Supercomplex dynamics in
721 response to light in *Chlamydomonas reinhardtii*. doi: 10.1101/2020.02.26.966580
722 **Chua NH, Bennoun P** (1975) Thylakoid membrane polypeptides of Chlamydomonas
723 reinhardtii: wild-type and mutant strains deficient in photosystem II reaction center.
724 Proc Natl Acad Sci **72**: 2175–2179
725 **Colina F, Carbó M, Meijón M, Cañal MJ, Valledor L** (2020) Low UV-C stress modulates
726 Chlamydomonas reinhardtii biomass composition and oxidative stress response
727 through proteomic and metabolomic changes involving novel signalers and
728 effectors. Biotechnol Biofuels **13**: 110
729 **Collaborative Computational Project, Number 4** (1994) The CCP4 suite: programs for
730 protein crystallography. Acta Crystallogr D Biol Crystallogr **50**: 760–763
731 **Concordet J-P, Haeussler M** (2018) CRISPOR: intuitive guide selection for
732 CRISPR/Cas9 genome editing experiments and screens. Nucleic Acids Res **46**:
733 W242–W245
734 **Criscuolo A, Gribaldo S** (2010) BMGE (Block Mapping and Gathering with Entropy): a
735 new software for selection of phylogenetic informative regions from multiple
736 sequence alignments. BMC Evol Biol **10**: 210
737 **Dahlgren KK, Gates C, Lee T, Cameron JC** (2021) Proximity-based proteomics reveals
738 the thylakoid lumen proteome in the cyanobacterium Synechococcus sp. PCC
739 7002. Photosynth Res **147**: 177–195
740 **Didaran F, Kordrostami M, Ghasemi-Soloklui AA, Pashkovskiy P, Kreslavski V,**
741 **Kuznetsov V, Allakhverdiev SI** (2024) The mechanisms of photoinhibition and
742 repair in plants under high light conditions and interplay with abiotic stressors. J
743 Photochem Photobiol B **259**: 113004

744 **Eletsky A, Acton TB, Xiao R, Everett JK, Montelione GT, Szyperski T** (2012) Solution
745 NMR structures reveal a distinct architecture and provide first structures for protein
746 domain family PF04536. J Struct Funct Genomics **13**: 9–14
747 **Emsley P, Cowtan K** (2004) Coot: model-building tools for molecular graphics. Acta
748 Crystallogr D Biol Crystallogr **60**: 2126–2132
749 **Fu A, He Z, Cho HS, Lima A, Buchanan BB, Luan S** (2007) A chloroplast cyclophilin
750 functions in the assembly and maintenance of photosystem II in *Arabidopsis*
751 *thaliana*. Proc Natl Acad Sci **104**: 15947–15952
752 **Gollan PJ, Trotta A, Bajwa AA, Mancini I, Aro E-M** (2021) Characterization of the Free
753 and Membrane-Associated Fractions of the Thylakoid Lumen Proteome in
754 Arabidopsis thaliana. Int J Mol Sci **22**: 8126
755 **Gopalan G, He Z, Balmer Y, Romano P, Gupta R, Héroux A, Buchanan BB,**
756 **Swaminathan K, Luan S** (2004) Structural analysis uncovers a role for redox in
757 regulating FKBP13, an immunophilin of the chloroplast thylakoid lumen. Proc Natl
758 Acad Sci U S A **101**: 13945–13950
759 **Hall M, Mata-Cabana A, Åkerlund H, Florencio FJ, Schröder WP, Lindahl M,**
760 **Kieselbach T** (2010) Thioredoxin targets of the plant chloroplast lumen and their
761 implications for plastid function. PROTEOMICS **10**: 987–1001
762 **Hallgren J, Tsirigos KD, Pedersen MD, Almagro Armenteros JJ, Marcatili P, Nielsen**
763 **H, Krogh A, Winther O** (2022) DeepTMHMM predicts alpha and beta
764 transmembrane proteins using deep neural networks. doi:
765 10.1101/2022.04.08.487609
766 **Hao Y, Chu J, Shi L, Ma C, Hui L, Cao X, Wang Y, Xu M, Fu A** (2021) Identification of
767 interacting proteins of Arabidopsis cyclophilin38 (AtCYP38) via multiple screening
768 approaches reveals its possible broad functions in chloroplasts. J Plant Physiol **264**:
769 153487
770 **Harris EH** (1989) The Chlamydomonas sourcebook: a comprehensive guide to biology
771 and laboratory use. Academic Press, San Diego
772 **He Z, Li L, Luan S** (2004) Immunophilins and Parvulins. Superfamily of Peptidyl Prolyl
773 Isomerases in Arabidopsis. Plant Physiol **134**: 1248–1267
774 **Heinnickel ML, Grossman AR** (2013) The GreenCut: re-evaluation of physiological role
775 of previously studied proteins and potential novel protein functions. Photosynth Res
776 **116**: 427–436
777 **Hoang DT, Chernomor O, von Haeseler A, Minh BQ, Vinh LS** (2018) UFBoot2:
778 Improving the Ultrafast Bootstrap Approximation. Mol Biol Evol **35**: 518–522

Hoh D, Froehlich JE, Kramer DM (2024) Redox regulation in chloroplast thylakoid lumen: The *pmf* changes everything, again. Plant Cell Environ **47**: 2749–2765

Hohmann-Marriott MF, Blankenship RE (2011) Evolution of photosynthesis. Annu Rev Plant Biol **62**: 515–548

Järvi S, Gollan PJ, Aro E-M (2013) Understanding the roles of the thylakoid lumen in photosynthesis regulation. Front Plant Sci **4**: 434

Kalyaanamoorthy S, Minh BQ, Wong TKF, Von Haeseler A, Jermiin LS (2017) ModelFinder: fast model selection for accurate phylogenetic estimates. Nat Methods **14**: 587–589

Katoh K, Standley DM (2013) MAFFT multiple sequence alignment software version 7: improvements in performance and usability. Mol Biol Evol **30**: 772–780

Keegan RM, Winn MD (2007) Automated search-model discovery and preparation for structure solution by molecular replacement. Acta Crystallogr D Biol Crystallogr **63**: 447–457

Kelterborn S, Boehning F, Sizova I, Baidukova O, Evers H, Hegemann P (2022) Gene Editing in Green Alga Chlamydomonas reinhardtii via CRISPR-Cas9 Ribonucleoproteins. Methods Mol Biol Clifton NJ **2379**: 45–65

Khrustaleva TA (2014) Secondary structure preferences of mn (2+) binding sites in bacterial proteins. Adv Bioinforma **2014**: 501841

Lemeille S, Willig A, Depège-Fargeix N, Delessert C, Bassi R, Rochaix J-D (2009) Analysis of the Chloroplast Protein Kinase Stt7 during State Transitions. PLoS Biol **7**: e1000045

Li X, Patena W, Fauser F, Jinkerson RE, Saroussi S, Meyer MT, Ivanova N, Robertson JM, Yue R, Zhang R, et al (2019) A genome-wide algal mutant library and functional screen identifies genes required for eukaryotic photosynthesis. Nat Genet **51**: 627–635

Lindahl M, Kieselbach T (2009) Disulphide proteomes and interactions with thioredoxin on the track towards understanding redox regulation in chloroplasts and cyanobacteria. J Proteomics **72**: 416–438

Lu Y, Du J-J, Yu Z-B, Peng J-J, Xu J-N, Wang X-Y (2015) Identification of Potential Targets for Thylakoid Oxidoreductase AtVKOR/LTO1 in Chloroplasts. Protein Pept Lett **22**: 219–225

McCann SD, Stahl SS (2015) Copper-Catalyzed Aerobic Oxidations of Organic Molecules: Pathways for Two-Electron Oxidation with a Four-Electron Oxidant and a One-Electron Redox-Active Catalyst. Acc Chem Res **48**: 1756–1766

Merchant SS, Prochnik SE, Vallon O, Harris EH, Karpowicz SJ, Witman GB, Terry A, Salamov A, Fritz-Laylin LK, Maréchal-Drouard L, et al (2007) The *Chlamydomonas* Genome Reveals the Evolution of Key Animal and Plant Functions. Science **318**: 245–250

Minh BQ, Schmidt HA, Chernomor O, Schrempf D, Woodhams MD, von Haeseler A, Lanfear R (2020) IQ-TREE 2: New Models and Efficient Methods for Phylogenetic Inference in the Genomic Era. Mol Biol Evol **37**: 1530–1534

Mulkidjanian AY, Koonin EV, Makarova KS, Mekhedov SL, Sorokin A, Wolf YI, Dufresne A, Partensky F, Burd H, Kaznadzey D, et al (2006) The cyanobacterial genome core and the origin of photosynthesis. Proc Natl Acad Sci U S A **103**: 13126–13131

Murshudov GN, Vagin AA, Lebedev A, Wilson KS, Dodson EJ (1999) Efficient anisotropic refinement of macromolecular structures using FFT. Acta Crystallogr D Biol Crystallogr **55**: 247–255

Naito Y, Hino K, Bono H, Ui-Tei K (2015) CRISPRdirect: software for designing CRISPR/Cas guide RNA with reduced off-target sites. Bioinforma Oxf Engl **31**: 1120–1123

Pellizza LA, Smal C, Ithuralde RE, Turjanski AG, Cicero DO, Arán M (2016) Structural and functional characterization of a cold-adapted stand-alone TPM domain reveals a relationship between dynamics and phosphatase activity. FEBS J **283**: 4370–4385

Pérez-Pérez ME, Mauriès A, Maes A, Tourasse NJ, Hamon M, Lemaire SD, Marchand CH (2017) The Deep Thioredoxome in Chlamydomonas reinhardtii: New Insights into Redox Regulation. Mol Plant **10**: 1107–1125

Porra RJ, Thompson WA, Kriedemann PE (1989) Determination of accurate extinction coefficients and simultaneous equations for assaying chlorophylls a and b extracted with four different solvents: verification of the concentration of chlorophyll standards by atomic absorption spectroscopy. Biochim Biophys Acta BBA - Bioenerg **975**: 384–394

Riché A, Dumas L, Malesinski S, Bossan G, Madigou C, Zito F, Alric J (2024) The stromal side of the cytochrome b6f complex regulates state transitions. Plant Cell koae190

Shapiguzov A, Edvardsson A, Vener AV (2006) Profound redox sensitivity of peptidyl-prolyl isomerase activity in Arabidopsis thylakoid lumen. FEBS Lett **580**: 3671–3676

848 **Sinha A, Eniyan K, Sinha S, Lynn AM, Bajpai U** (2015) Functional analysis of TPM
849 domain containing Rv2345 of Mycobacterium tuberculosis identifies its
850 phosphatase activity. Protein Expr Purif **111**: 23–27
851 **Sirpiö S, Allahverdiyeva Y, Suorsa M, Paakkarinen V, Vainonen J, Battchikova N, Aro**
852 **E-M** (2007) TLP18.3, a novel thylakoid lumen protein regulating photosystem II
853 repair cycle. Biochem J **406**: 415–425
854 **Sirpiö S, Khrouchtchova A, Allahverdiyeva Y, Hansson M, Fristedt R, Vener AV,**
855 **Scheller HV, Jensen PE, Haldrup A, Aro E** (2008) AtCYP38 ensures early
856 biogenesis, correct assembly and sustenance of photosystem II. Plant J **55**: 639–
857 651
858 **Vasudevan D, Fu A, Luan S, Swaminathan K** (2012) Crystal structure of Arabidopsis
859 cyclophilin38 reveals a previously uncharacterized immunophilin fold and a
860 possible autoinhibitory mechanism. Plant Cell **24**: 2666–2674
861 **Vidal-Meireles A, Horrenberger Y, Malesinski S, Siponen M, Monteil C, Bergot M,**
862 **Alric J, Johnson X** (2024) The potential role of TLP15.2 during high light
863 acclimation in Chlamydomonas reinhardtii.
864 **Vidal-Meireles A, Neupert J, Zsigmond L, Rosado-Souza L, Kovács L, Nagy V,**
865 **Galambos A, Fernie AR, Bock R, Tóth SZ** (2017) Regulation of ascorbate
866 biosynthesis in green algae has evolved to enable rapid stress-induced response
867 via the VTC2 gene encoding GDP-l-galactose phosphorylase. New Phytol **214**:
868 668–681
869 **Wang L, Patena W, Van Baalen KA, Xie Y, Singer ER, Gavrilenko S, Warren-Williams**
870 **M, Han L, Harrigan HR, Hartz LD, et al** (2023) A chloroplast protein atlas reveals
871 punctate structures and spatial organization of biosynthetic pathways. Cell **186**:
872 3499-3518.e14
873 **Wegener KM, Bennewitz S, Oelmüller R, Pakrasi HB** (2011) The Psb32 protein aids in
874 repairing photodamaged photosystem II in the cyanobacterium Synechocystis
875 6803. Mol Plant **4**: 1052–1061
876 **Wu HY, Liu MS, Lin TP, Cheng YS** (2011) Structural and functional assays of AtTLP18.3
877 identify its novel acid phosphatase activity in thylakoid lumen. Plant Physiol **157**:
878 1015–1025
879 **Wu J, Rong L, Lin W, Kong L, Wei D, Zhang L, Rochaix J-D, Xu X** (2021) Functional
880 redox links between lumen thiol oxidoreductase1 and serine/threonine-protein
881 kinase STN7. Plant Physiol **186**: 964–976

Yu J, Baek K, Jin E, Bae S (2017) DNA-free Genome Editing of Chlamydomonas reinhardtii Using CRISPR and Subsequent Mutant Analysis. BIO-Protoc. doi: 10.21769/BioProtoc.2352

Zones JM, Blaby IK, Merchant SS, Umen JG (2015) High-Resolution Profiling of a Synchronized Diurnal Transcriptome from Chlamydomonas reinhardtii Reveals Continuous Cell and Metabolic Differentiation. Plant Cell **27**: 2743–2769

Accession numbers

Sequence data for the proteins referred in this article can be found in Uniprot under the following accession numbers: LMTP1: A8JDW2_CHLRE; TLP26: A0A2K3DVX2_CHLRE; Sll1071: P73281_SYNY3; AT5G52970: TL15B_ARATH; CrTLP18.3: A8JH60_CHLRE. The coordinates of the recombinant LMTP1 crystal were deposited on the RCSB Protein Data Bank (RCSB PDB) under the PDB ID 9H70.

List of Figures

Figure 1: Generation of *C. reinhardtii ΔlmPt1* and *Δtlp26* mutants via CRISPR/Cas9.
Figure 2: LMTP1 and TLP26 protein accumulation increases during acclimation to photoautotrophic conditions; mutants are phototrophic under non-stressful conditions.
Figure 3: Crystal structure of recombinant CrLMTP1.
Figure 4: Recombinant CrLMTP1 shows binding to manganese (Mn^{2+}) and its thermal stability increases under reducing conditions.
Figure 5: Recombinant LMTP1 and TLP26 exhibit very low phosphatase activity.
Figure 6: Maximum likelihood unrooted tree of the TPM-domain family (PANTHER entry PTHR35514 / Thylakoid_lumenal_15kDa-like) showing its distribution in green and red algae, land plants and cyanobacteria.

Supplemental Figure 1: Predicted structures of different TPM-domain containing proteins and their modelled interactions with divalent metals.
Supplemental Figure 2: Alignment of the mature protein sequences of CrLMTP1, AtLMTP1, Sll1071, CrTLP26, and CrTLP18.3.

915 Supplemental Figure 3: Maximum likelihood rooted tree of the TPM-domain family
916 (PANTHER entry PTHR35514 / Thylakoid_lumenal_15kDa-like) showing its distribution in
917 green and red algae, land plants and cyanobacteria.

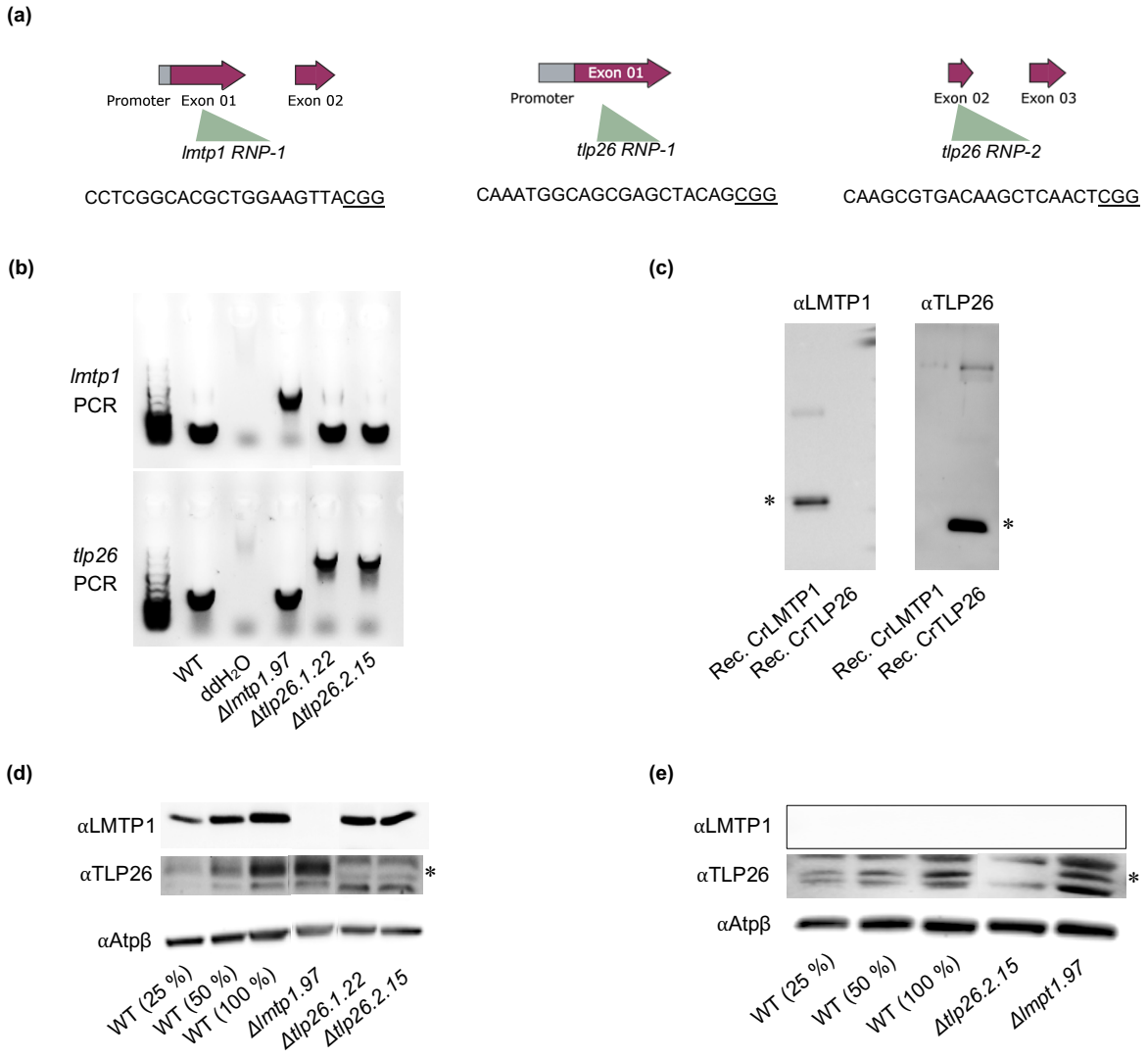

Figure 1 – Generation of *C. reinhardtii Δlmpt1* and *Δtlp26* mutants via CRISPR/Cas9. (a) Schematic representation of the 5' region of Cre15.g636050 (encoding LMTP1) and Cre03.g154600 (encoding TLP26) gene models, indicating the chosen PAM sites for the CRISPR/Cas9 knock-out mutants generated. **(b)** PCR fragments using specific primers spanning the CRISPR target sites, confirming the presence of a large insertion (> 1 kbp) within the target genes of selected mutants. **(c)** Immunoblot analysis of recombinant CrLMTP1 and truncated (i.e. only soluble/TPM domain – see Supplemental Figure 2) CrTLP26 proteins, showing that the antibodies recognize their specific recombinant protein. **(d)** Immunoblot analysis of different *C. reinhardtii* strains, showing that the CRISPR/Cas9 mutants cannot accumulate LMTP1 or TLP26, as well as the antibody specificity. **(e)** Immunoblot analysis of thylakoid membranes from different *C. reinhardtii* strains, showing TLP26 signal and no LMPT1 detection. Anti-Atpβ was used as a loading control; 100 % corresponds to 1 µg Chl (*a*+*b*). * indicates the expected protein migration band.

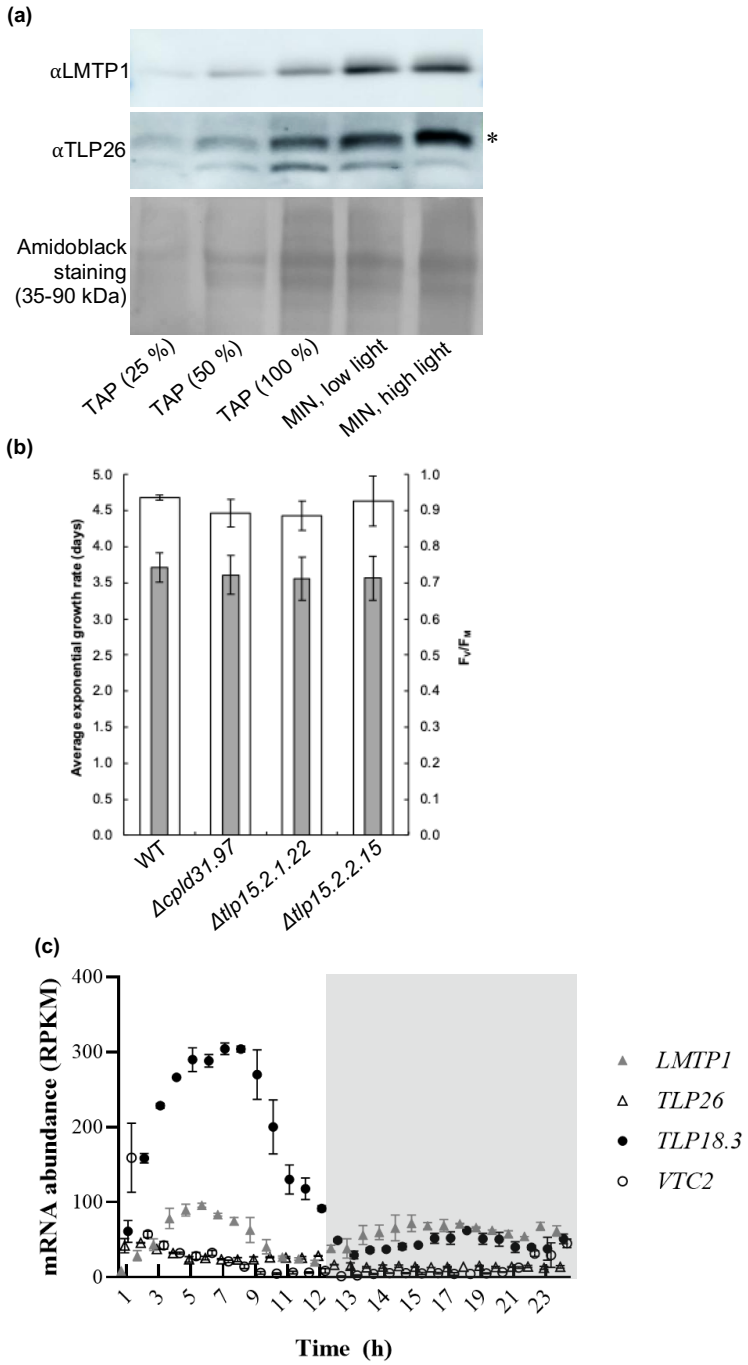

Figure 2 – LMTP1 and TLP26 protein accumulation increases during acclimation to photoautotrophic conditions; mutants are phototrophic under non-stressful conditions. (a) Immunoblot analysis of the acclimation of *C. reinhardtii* wild-type cells from photomixotrophic conditions (TAP medium) to photoautotrophic growth (MIN medium), first under low light (40 µmol photons·m^{-2}·s^{-1}), and then under high light (250 µmol photons·m^{-2}·s^{-1}) constant illumination, showing the accumulation of LMTP1 and TLP26; 100 % corresponds to 1 µg Chl (a+b); * indicates the expected protein migration band; the amidoblack staining corresponds to the upper fraction of the blotted membraned (35-90 kDa). **(b)** Exponential doubling time (white bars) and F_V/F_M Chl *a* fluorescence parameter (gray bars) of different *C. reinhardtii* strains acclimated to photoautotrophic growth under low light constant light intensity. Data is represented as mean ± standard deviation (n = 3 biological replicates). **(c)** Circadian regulation of the mRNA abundance of *LMTP1* (Cre15.g636050) and *TLP26* (Cre03.g154600), in comparison with *TLP18.3* (Cre03.g182150) and *VTC2* (Cre13.g588150); data was obtained from (Zones et al., 2015) and represented as reads per kilobase of exon model per million mapped reads (RPKM).

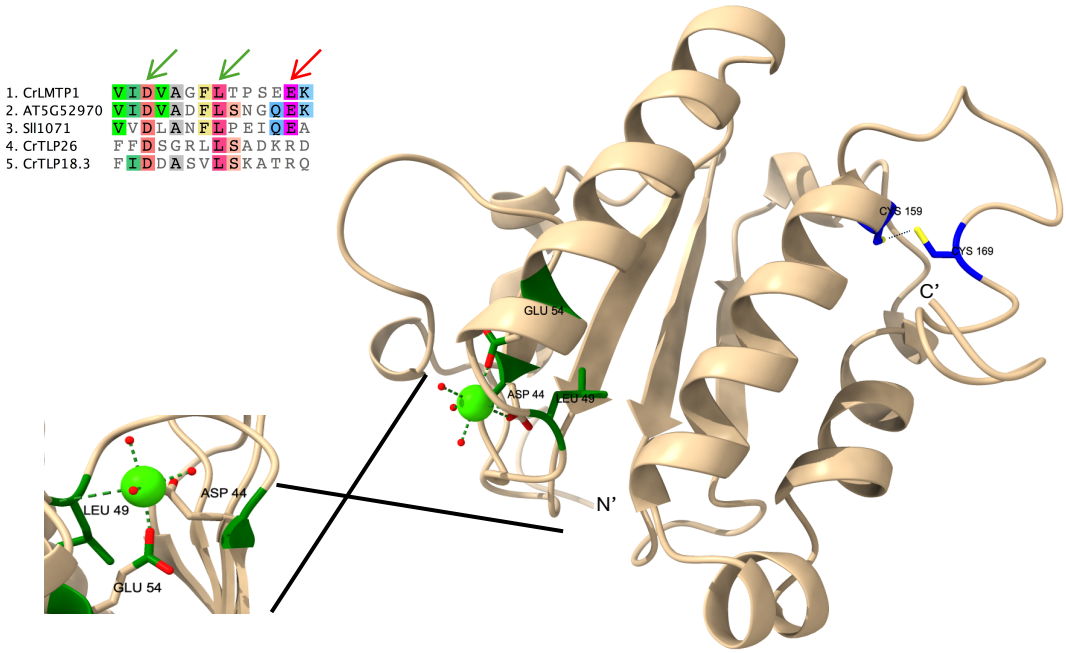

Figure 3 – Crystal structure of recombinant CrLMTP1. The crystal structure of the recombinant protein, resolved to 1.6 Å, showed the presence of a TPM-domain fold and revealed a metal-binding site at one of the N-terminus loops of the protein, hexa-coordinated, and interacting with the recombinant protein residues Asp44, Leu49, and Glu54. At the protein C-terminus, the cysteine pair forms an intra-molecular disulfide bridge. The inset shows the conservation of the coordination residues between homologues of LMTP1 in different species against CrTLP26 and TLP18.3 from *C. reinhardtii*, where the green arrows show amino acids conserved in all of the TPM domain proteins and the red arrow shows that Glu54 is only conserved in LMTP homologues.

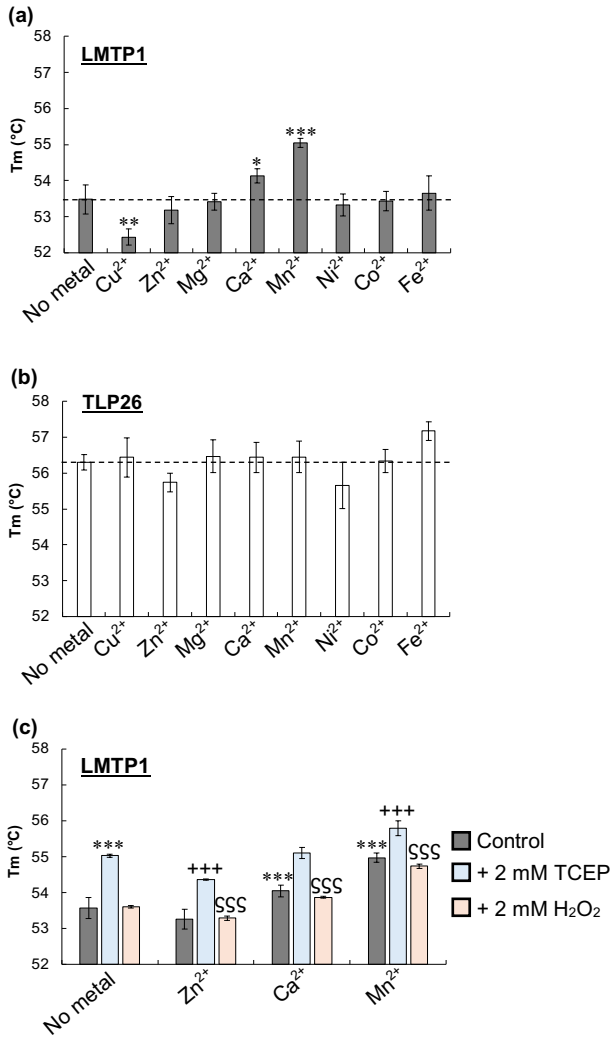

Figure 4 – Recombinant CrLMTP1 shows binding to manganese (Mn^{2+}) and its thermal stability increases under reducing conditions. Nano-DSF thermal denaturation assays for recombinant **(a)** LMTP1 or **(b)** TLP26, showing variations in the protein melting temperature (Tm) upon incubation with 5 molar equivalents of different divalent metals. **(c)** Denaturation assays for LMTP1 incubated under reduced (+ TCEP) or oxidized (+ H_2O_2) conditions in the absence or presence of 5 molar equivalents of the selected divalent metals. Data is represented as mean ± standard deviation (n = 3 replicates). Statistical significance was determined by one-way ANOVA test (* shows statistical significance vs. "LMTP1 No metal", + shows statistical significance vs. "LMTP1 + 2 mM TCEP", and ς shows statistical significance vs. "LMTP1 + 2mM H_2O_2).

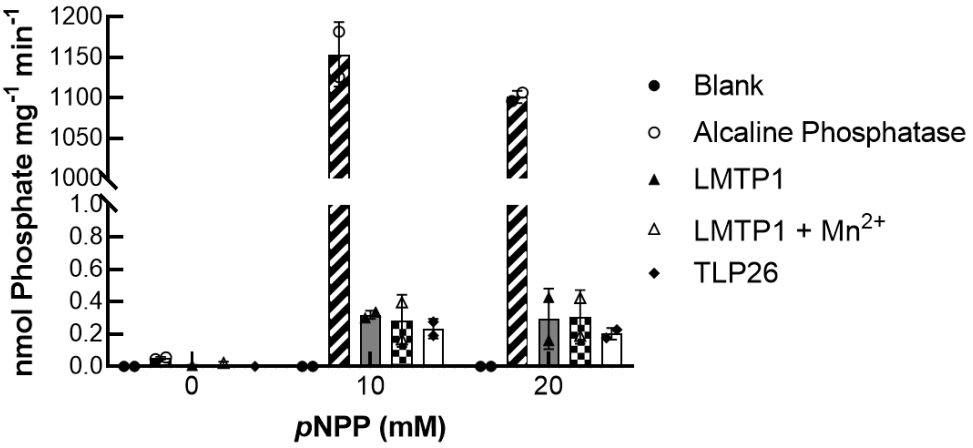

Figure 5 – Recombinant LMTP1 and TLP26 exhibit very low phosphatase activity. Rate of phosphate release evaluated by colorimetric assay upon incubation of the recombinant proteins with different concentrations of the non-specific substrate *p*NPP; as a positive control, Alkaline Phosphatase (Sigma-Aldrich) was used. Data is represented as mean ± standard deviation (n = 2 replicates).

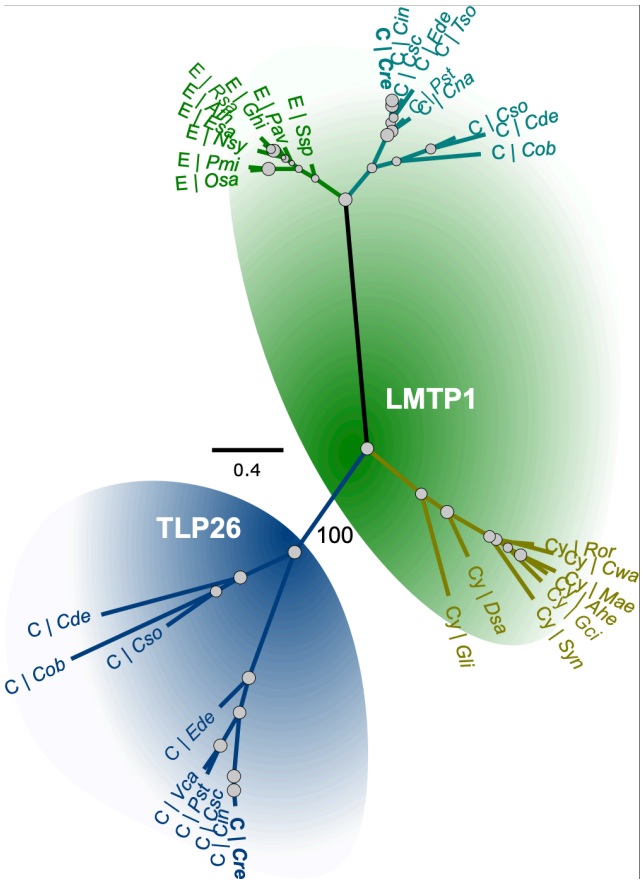

Figure 6 – Maximum likelihood unrooted tree of the TPM-domain family (PANTHER entry PTHR35514 / Thylakoid_lumenal_15kDa-like) showing its distribution in green and red algae, land plants and cyanobacteria. Unrooted tree with green *Chlorophyta* (C), *Cyanobacteriota* (Cy) and *Embryophyta* (E) clades. The first three letters of the acronyms indicate the species (*Ahe, Aphanothece hegewaldii; Ath, Arabidopsis thaliana; Cde, Chlorella desiccata; Cin, Chlamydomonas incerta; Cob, Coccomyxa sp.; Cre, Chlamydomonas reinhardtii; Csc, Chlamydomonas schloesseri; Cso, Chlorella sorokiniana; Cwa, Crocosphaera watsonii; Dsa, Dactylococcopsis salina; Ede, Edaphochlamys debaryana; Esa, Eutrema salsugineum; Gci, Gloeothece citriformis; Ghi, Gossypium hirsutum; Gli,; Mae, Microcystis aeruginosa; Nsy, Nicotiana sylvestris; Osa, Oryza sativa; Pav, Prunus avium; Pim, Panicum miliaceum; Ror, Rippkaea orientalis; Pst, Pleodorina starrii; Rsa, Raphanus sativus; Ssp, Salvia splendens; Syn, Synechocystis sp.; Tso, Tetrabaena socialis; Vca, Volvox carteri).* Accessions numbers are given in Figure S3. The tree was drawn to scale and the scale bar represents the number of substitutions per site. Tree topology was tested using an ultrafast bootstrap approximation approach with 1000 replicates; gray circles represent bootstrap values and are drawn to scale.